# Electronic Supplementary Information

# Constructing POSS and viologen-linked porous cationic frameworks induced by the Zincke reaction for efficient $CO_2$ capture and conversion

Guojian Chen,*[a] Xiaohui Huang,[a] Yadong Zhang,[a] Mengyao Sun,[a] Jie Shen,[a] Rui Huang,[a] Minman Tong,[a] Zhouyang Long*[a] and Xiaochen Wang[b]

[a] School of Chemistry and Materials Science, Jiangsu Key Laboratory of Green Synthetic Chemistry for Functional Materials, Jiangsu Normal University, Xuzhou 221116, China

[b] Department of Chemistry and Materials Engineering, Hefei University, Hefei 230022, China

* Corresponding author:

E-mail: gjchen@jsnu.edu.cn (G. J. Chen); longzhouyangfat@163.com (Z. Y. Long)

# Experimental Section

## Materials

Octa(aminophenyl)silsesquioxane ($NH_2$-POSS, HWRK), 4,4´-bipyridine (Adamas), 1-chloro-2,4-dinitrobenzene (Alfa), 1-bromo-2,4-dinitrobenzene (Alfa) and solvents N,N-Dimethylformamide (DMF), Dimethylacetamide (DMAc), N,N-Diethylformamide (DEF), Dimethyl sulfoxide (DMSO) and other common solvents were commercially available and used as received.

## Methods

Liquid-state $^{1}H$ and $^{13}C$ NMR spectra were measured with a Bruker DPX 500 spectrometer at ambient temperature in the solvent of $D_2O$ using TMS as internal reference. Solid-state $^{29}Si$ MAS NMR, $^{13}C$ and $^{1}H$ spin-echo pulse NMR spectra were carried out a Bruker AVANCE III 600 spectrometer at a resonance frequency of 119.2 MHz using a 4 mm HX double-resonance MAS probe. The CHN elemental analysis was performed on an elemental analyzer Vario EL cube. Fourier transform infrared spectroscopy (FTIR) was recorded on a Bruker Vertex 80V FTIR instrument (KBr discs) in the region 4,000-400 $cm^{-1}$. The Si-OH groups in samples were identified by *in situ* FTIR spectroscopy (Bruker, EQUINOX55) under vacuum condition at 200 $^{o}C$. Before testing, the samples were treated at 200 $^{o}C$ for 6 h under vacuum condition to remove the adsorbed water. Thermogravimetric analysis (TGA) was carried out with a TA Q50 instrument in nitrogen or air atmosphere at a heating rate of 10 $^{o}C$ $min^{-1}$. XRD patterns were collected on the Bruker D8 Advance powder diffractometer using Ni-filtered Cu Ka radiation source at 40 kV and 20 mA, from 5 to $80^{o}$ with a scan rate of $0.2^{o}$ $s^{-1}$. Field emission scanning electron microscope (FESEM, Hitachi SU8010) accompanied by Energy dispersive X-ray spectrometry (EDS) was used to study the morphology and the elements distribution. Transmission Electron Microscopy (TEM) images were obtained by using a JEOL JEM-2100F 200 kV field-emission transmission electron microscope. $N_2$ adsorption isotherms were measured at 77 K using a Quantachrome autosorb iQ2 analyzer, and the surface area of samples was calculated using the Brunauer-Emmett-Teller (BET) method and the pore size distribution was determined by nonlocal density functional theory (NLDFT) model ($N_2$ 77 K on carbon, slit pore) and Barrett-Joyner-Halenda (BJH) method. The $CO_2$ adsorption isotherms at 273 and 298 K were also measured using the Quantachrome autosorb iQ2 analyzer. All the samples were degassed at 150 ℃ for 10 h in high vacuum before the adsorption experiments for both $N_2$ and $CO_2$. The contents of $Cl^-$ and $Br^-$ anions were measured by a Dionex ICS-2000 ion chromatographic analyser (Dionex, USA). The surface chemical composition was determined by X-ray photoelectron spectroscopy (XPS, Thermo ESCALAB 250Xi, USA) using an X-ray source of mono-chromatic Al Ka (1486.6 eV) 150 W.

## Synthesis of viologen linkers

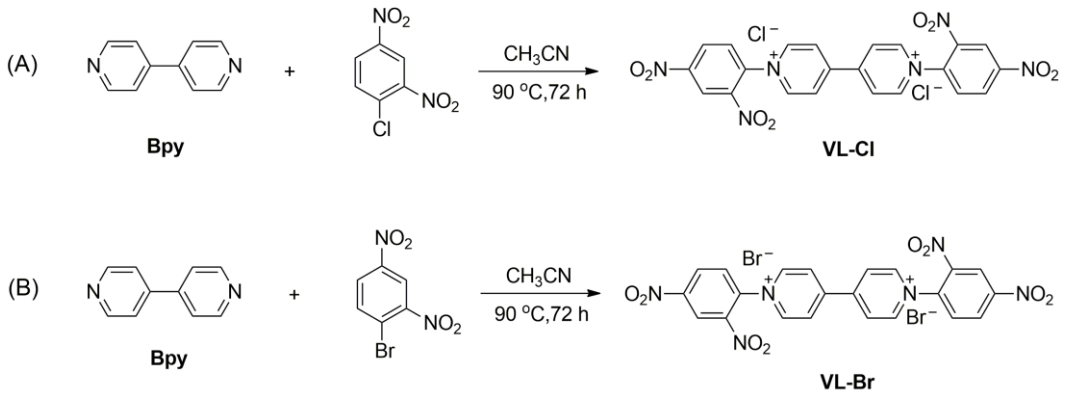


**Scheme S1** Synthesis of viologen linkers (A) VL-Cl and (B) VL-Br.

**Synthesis of VL-Cl:** As shown in Scheme S1A, 1,1'-bis(2,4-dinitrophenyl)-[4,4'-bipyridine]-1,1'-diium dichloride (denoted as VL-Cl) was prepared following previously reported literature procedure with a little modify.[S1] 4,4'-bipyridine (4.46 g, 30 mmol) and 1-chloro-2,4-dinitrobenzene (18.23 g, 90 mmol) were dissolved in $CH_3CN$ (100 mL). The reaction mixture was stirred under air atmosphere at 90 $^oC$ for 72 h. The final suspension was filtered and subsequently washed with $CH_3CN$ (3×20 mL) and then the resulting yellow powder was dried under vacuum at 80 $^oC$ for 12 h to give the product VL-Cl (10.10 g, yield of 60 %). VL-Cl: $^1H$ NMR (400 MHz, $D_2O$, Fig. S1A): $\delta$ 9.45~9.46 (CH, 4H), 9.37 (CH, 2H), 8.90~8.93 (CH, 6H) and 8.28~8.30 ppm (CH, 2H). $^{13}C$ NMR (100 MHz, $D_2O$, Fig. S1B): $\delta$ 152.64, 149.86, 146.86, 142.81, 138.25, 131.16, 130.76, 127.58 and 122.81 ppm. Elemental analysis: Found: C, 46.69; H, 2.89; N, 14.74 wt%. Calcd. For $C_{22}H_{14}O_8N_6Cl_2$ (M.W. 561.29 ): C, 47.08; H, 2.51; N, 14.97 wt%.

**Synthesis of VL-Br:** As shown in Scheme S1B, 1,1'-bis(2,4-dinitrophenyl)-[4,4'-bipyridine]-1,1'-diium dibromide (denoted as VL-Br) was prepared by using a similar process with VL-Cl. 4,4'-bipyridine (4.46 g, 30 mmol) and 1-bromo-2,4-dinitrobenzene (22.23 g, 90 mmol) were dissolved in $CH_3CN$ (100 mL). The reaction mixture was stirred under air atmosphere at 90 $^oC$ for 72 h. The final suspension was filtered and subsequently washed with $CH_3CN$ (3×20 mL) and then the resulting yellow powder was dried under vacuum at 80 $^oC$ for 12 h to give the product VL-Br (16.35 g, yield of 85 %). VL-Br: $^1H$ NMR (400 MHz, $D_2O$, Fig. S2A): $\delta$ 9.41~9.42 (CH, 4H), 9.33~9.34 (CH, 2H), 8.86~8.89 (CH, 6H) and 8.24~8.26 ppm (CH, 2H). $^{13}C$ NMR (100 MHz, $D_2O$, Fig. S2B ): $\delta$ 152.58, 149.81, 146.80, 142.77, 138.19, 131.11, 130.70, 127.54 and 122.77 ppm. Elemental analysis: Found: C, 40.85; H, 2.51; N, 12.83 wt%. Calcd. for $C_{22}H_{14}O_8N_6Br_2$ (M.W. 650.19 ): C, 40.64; H, 2.17; N, 12.93 wt%.

## Synthesis of POSS-based viologen-linked porous cationic frameworks

POSS-based viologen-linked porous cationic frameworks were synthesized *via* the Zincke reaction between $NH_2$-POSS and viologen linkers (Scheme S2 and Scheme S3). Typically, $NH_2$-POSS (0.058 g, 0.05 mmol) was dissolved in 5 mL DMF and VL-Br (0.13 g, 0.2 mmol) was homogeneously dispersed in 5 mL DMF with stirring for 30 min at room temperature. Then, the mixture suspension solution containing $NH_2$-POSS and VL-Br was moved into a 25 mL Teflon-lined autoclave, which was taken place at 180 $^{o}$C in a constant temperature oven for 48 h. After reaction, the obtained dark brown gel-like solid with a little brown solution was dispersed and stirred in 10 mL DMSO solution for 1 h in order to dissolve the residual raw materials and probable oligomers. The suspension was filtered, thoroughly washed with DMSO, THF, water and ethanol, respectively. Finally, the dark brown V-PCIF-Br (0.058 g, yield of 50 %) was obtained by drying in a vacuum at 80 ℃ for 12 h. Elemental analysis: Found: C, 45.59; H, 3.71; N, 8.89 wt%.

The optimized synthetic conditions of V-PCIF-Br were also investigated by using different solvents (DMF, DMAc, DEF, DMSO, ethanol/water, dioxane and acetonitrile), different molar ratios of $NH_2$-POSS to VL-Br, and different reaction temperatures (140 $^{o}$C, 160 $^{o}$C and 180 $^{o}$C). Besides, the other product V-PCIF-Cl with $Cl^-$ anions was also synthesized by the replace of VL-Br with VL-Cl under the same conditions.

## Catalytic conversion of $CO_2$ into cyclic carbonates

The catalytic $CO_2$ cycloaddition with epoxides into cyclic carbonates was performed at both low $CO_2$ pressure (1.0 MPa) and atmospheric conditions ($CO_2$ balloon).

The pressured reaction was carried out using a stainless steel autoclave (10 mL) equipped with a magnetic stirrer. In a typical run, the mixture of epoxide (5 mmol) and catalyst V-PICF-Br (0.05 g) was placed in the autoclave, which was flushed twice with $CO_2$ (0.1 MPa) in order to make the air discharge, and then charged with $CO_2$ to 1.0 MPa. The reactor was heated at 120 $^{o}$C for 6 h. After reaction, the reactor was cooled down to room temperature to slowly release the residue $CO_2$. Then, the internal standard *n*-dodecane was added and the resulting mixture was diluted with ethyl acetate. The conversion and selectivity were determined by a gas chromatography (GC) plus $^{1}$H NMR. The solid catalyst was separated by filtration, washed with ethyl acetate, dried in the vacuum and then was directly reused in the next run.

In a typical process of the reaction under atmospheric $CO_2$ conditions (0.1 MPa), epoxide (5 mmol) and V-PICF-Br (0.05 g) were placed in a Schlenk tube with $CO_2$ purged with a balloon and then the mixture was stirred at the targeted temperature. After reaction, the solid was removed by centrifugation, and the product was measured by GC and $^{1}$H NMR.

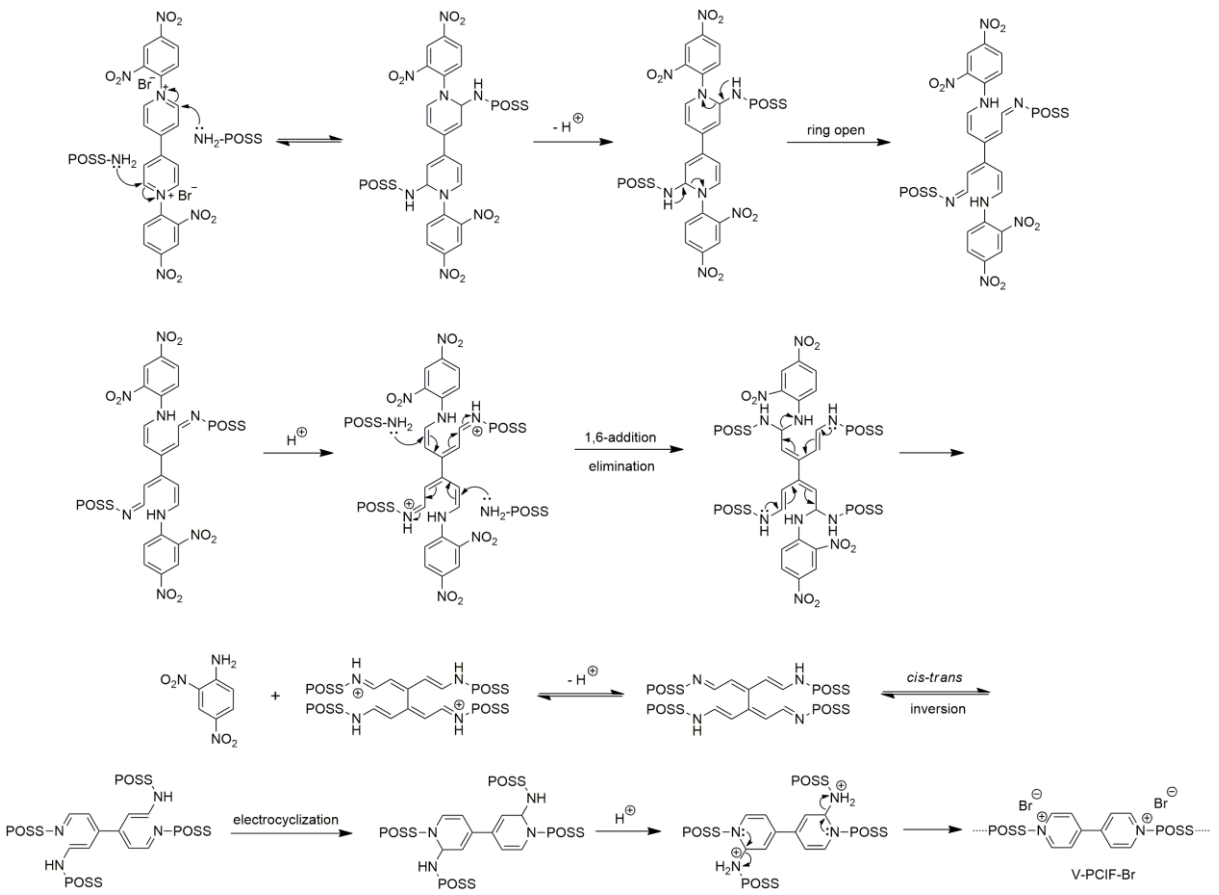


**Scheme S2** The detailed mechanisms of the Zincke reaction for the formation of V-PCIF-Br *via* a succession of nucleophilic attack, electrocyclic ring opening, electrocyclization and elimination of 2,4-dinitroaniline, in accordance with previous descriptions. (J.J. Li, Name Reactions: A Collection of Detailed Mechanisms and Synthetic Applications, DOI 10.1007/978-3-319-03979-4_299)

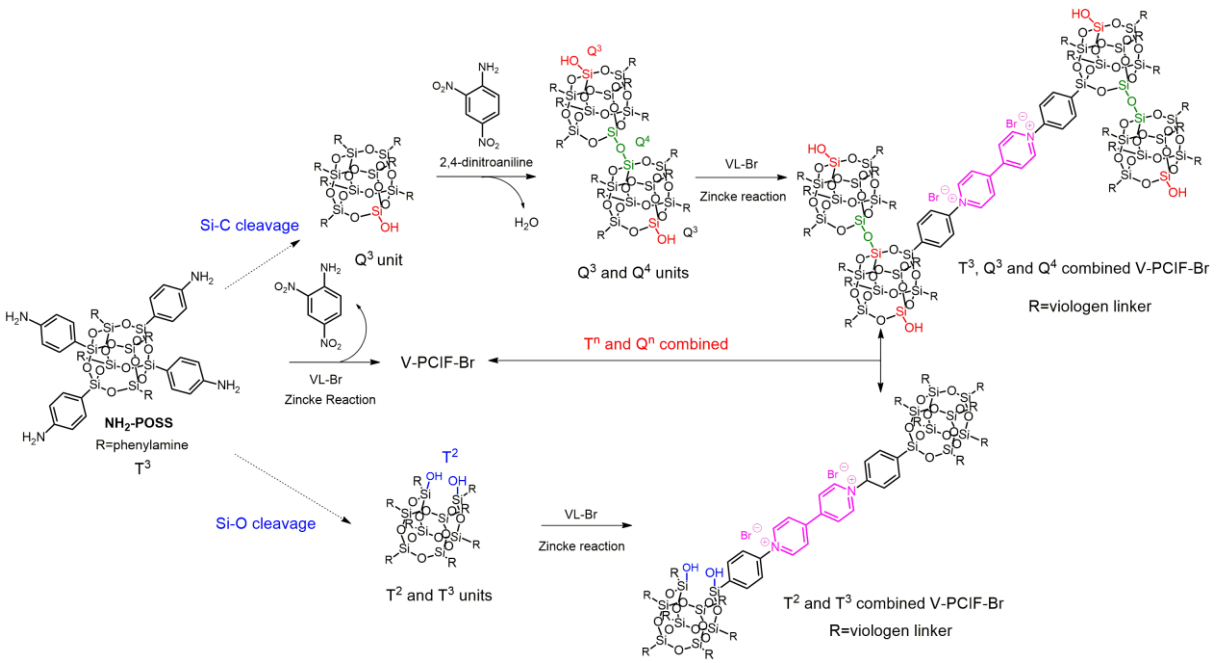


**Scheme S3** The formation process of $T^n$ and $Q^n$ units combined POSS and viologen-linked porous cationic framework V-PCIF-Br.

Scheme S3 depicts the detailed formation process of $T^n$ and $Q^n$ units combined POSS and viologen-linked porous cationic framework V-PCIF-Br. $Q^3$ units are formed due to the Si-C bonds cleavage of $T^3$ units, which are caused by the cross-linking of rigid viologen linkers and release of basic 2,4-dinitroaniline. One is ascribed to the distortion of cubic POSS cages when they are connected by rigid viologen linkers, the other is own to the basic 2,4-dinitroaniline that will break Si-C bonds. Besides, getting from the mechanism of the Zincke reaction (Scheme S2), the nucleophilic attack between $NH_2$-POSS and VL-Br will aggravate the cleavage of Si-C bonds in the present of the inevitable water.[S2,S3] Successively, the $Q^4$-structured POSS units are originated from the self-condensation of Si-OH from the obtained $Q^3$ units under the weak basic environment. A minor $T^2$ unit arises from partial Si-O cleavage of POSS cages, due to the spatial distortion of POSS cages cross-linked by rigid viologen moieties. During the Zincke reaction, $T^2$, $T^3$, $Q^3$ and $Q^4$ silicons coexist in the formed POSS-based porous cationic framework, which are confirmed by $^{29}$Si NMR and FTIR spectra. In a word, the formation process is initially induced by the Zincke reaction that is the nucleophilic attack between $NH_2$-POSS and rigid viologen linker, and then involves the successive reaction-triggered cleavage of Si-C bonds and further condensation of Si-OH, which together contribute to the formation of $T^n$ and $Q^n$ combined POSS and viologen-linked V-PCIF-Br. Obviously, the two coexisting viologen ionic linker and Si-O-Si linker in V-PCIF-Br work together to construct the porous skeleton, among which viologen ionic linker affords the ionic sites and $T^2$ and $Q^3$ units offer the desired Si-OH groups.

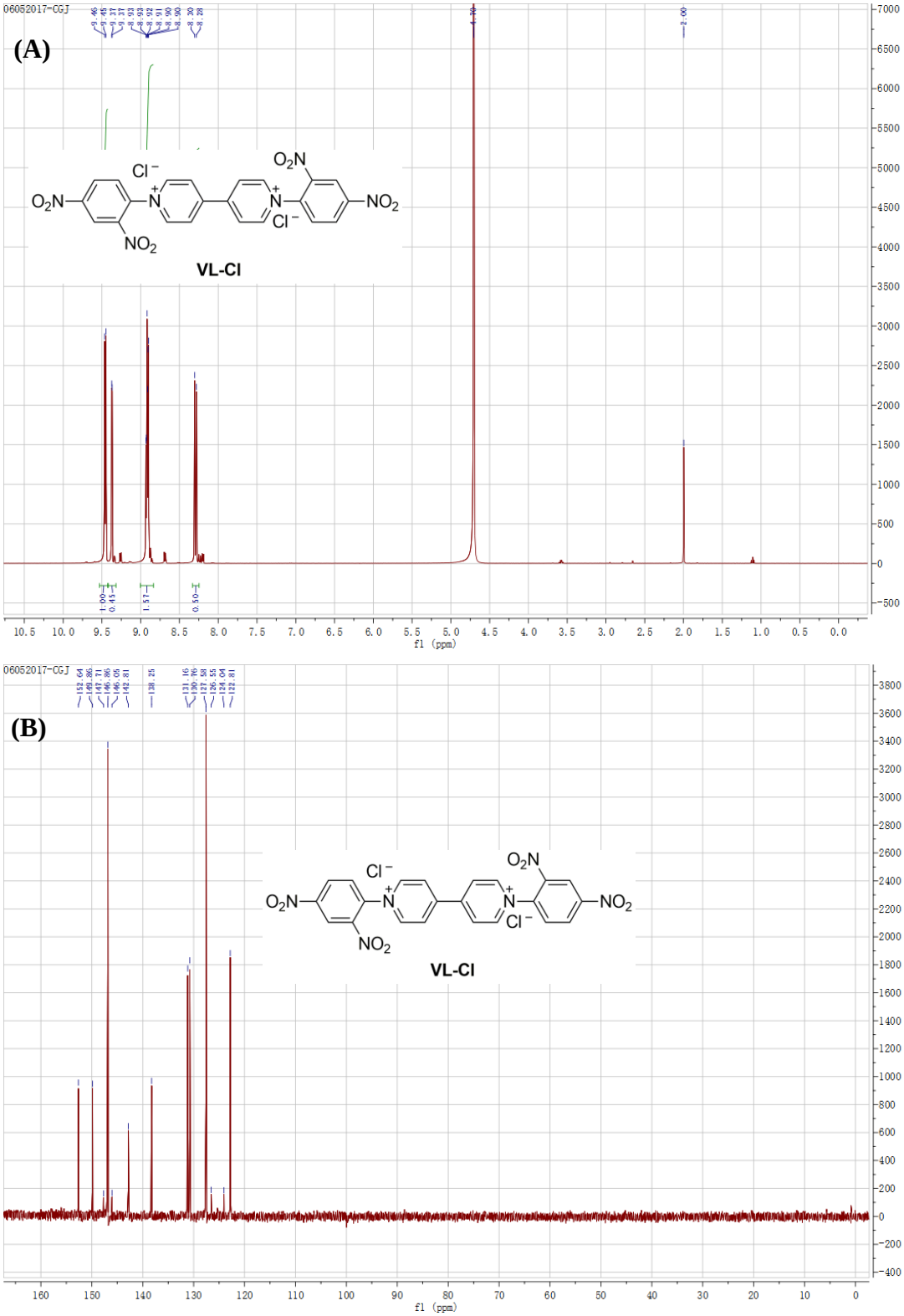


**Fig. S1** (A) $^{1}$H NMR and (B) $^{13}$C NMR of VL-Cl in the solvent $D_2O$.

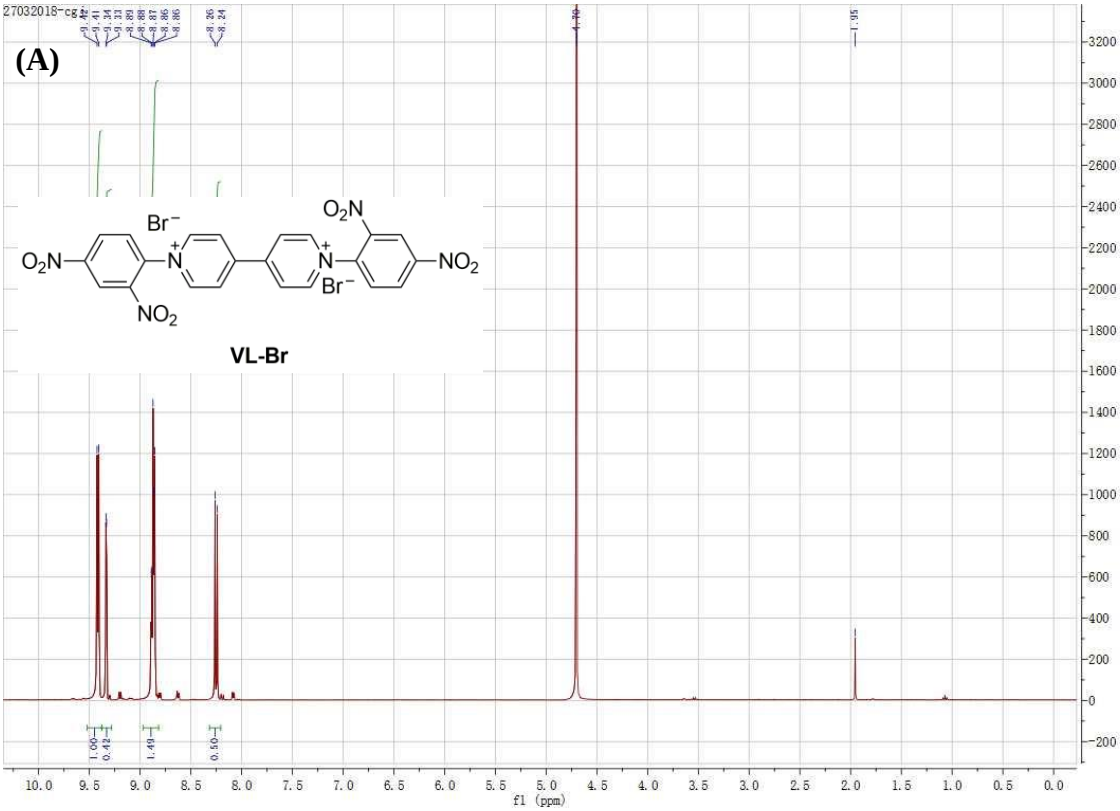


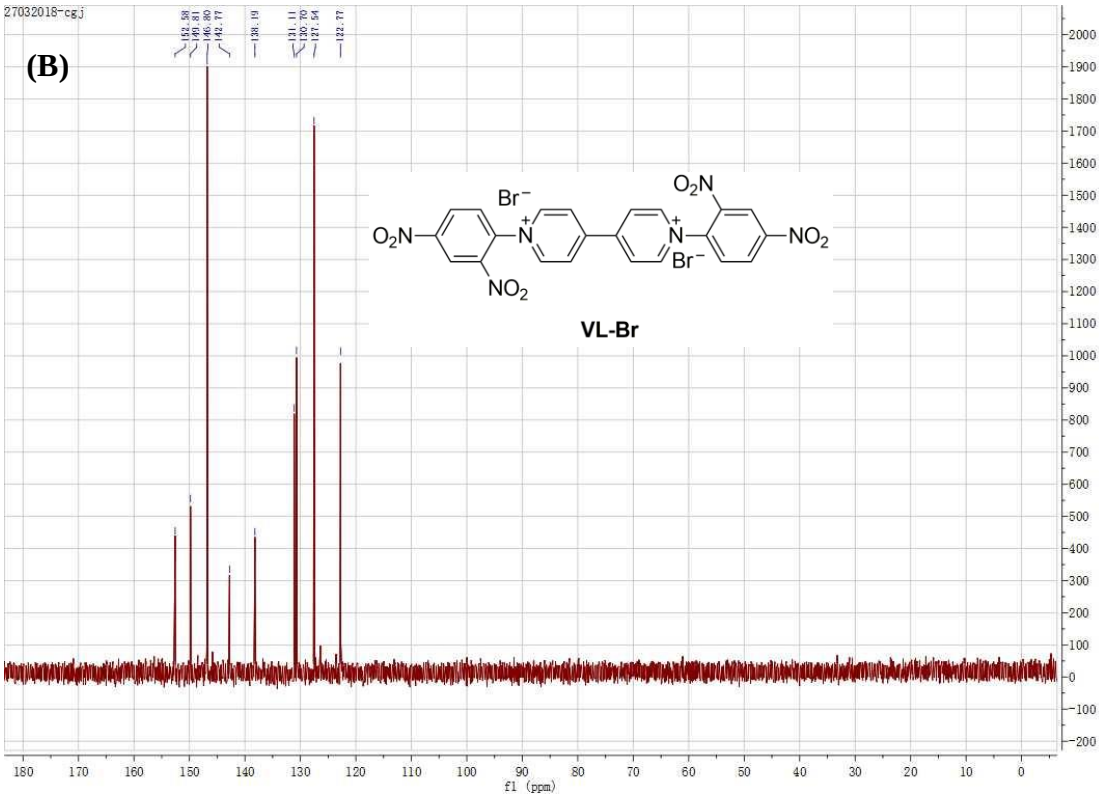


**Fig. S2** (A) $^{1}$H NMR and (B) $^{13}$C NMR of VL-Br in the solvent $D_2O$.

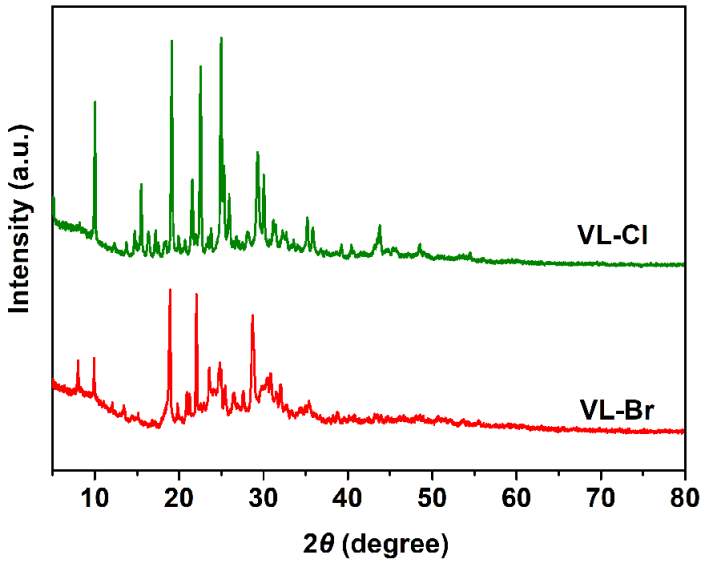


**Fig. S3** XRD patterns of VL-X (X=Cl, Br).

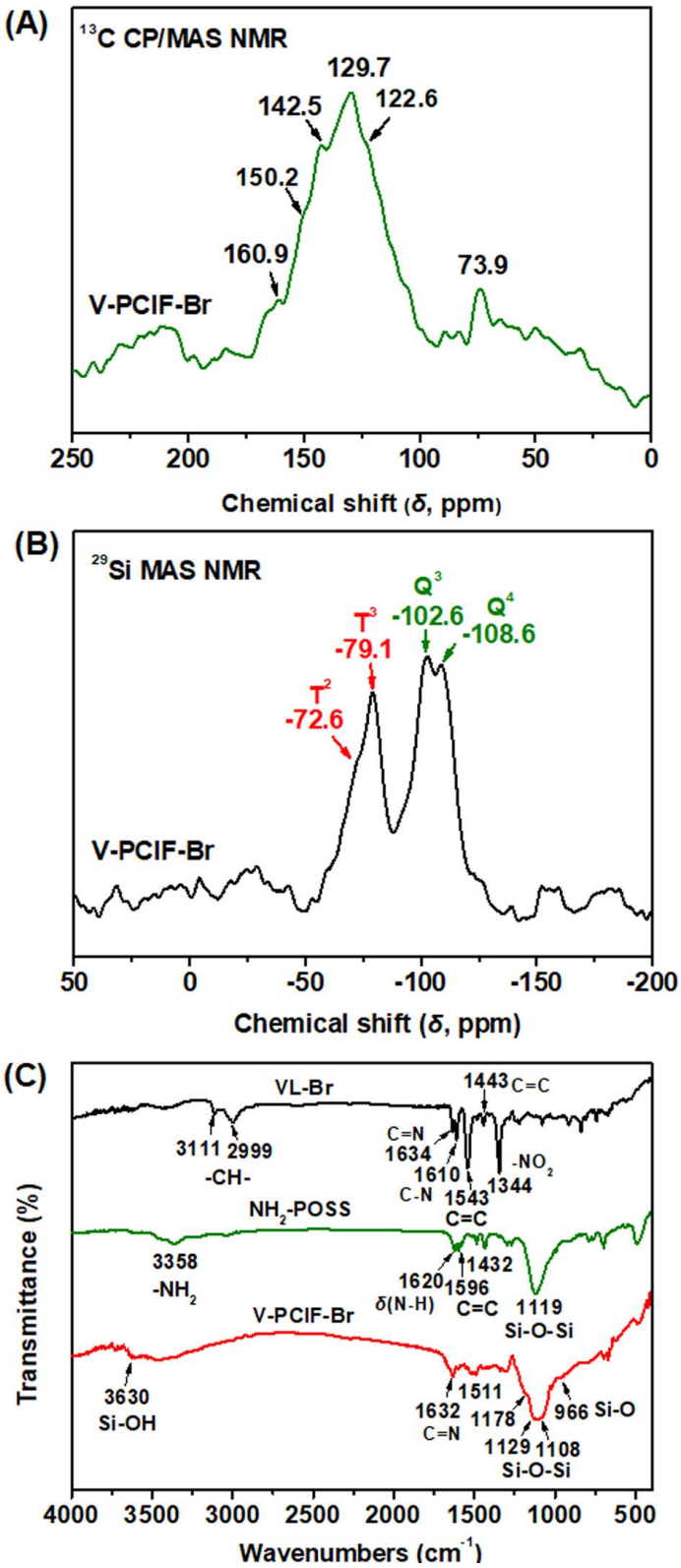


**Fig. S4** (A) $^{13}$C CP/MAS NMR spectrum and (B) $^{29}$Si MAS NMR spectrum of the typical sample V-PCIF-Br. (C) FTIR spectra of VL-Br, $NH_2$-POSS and V-PCIF-Br.

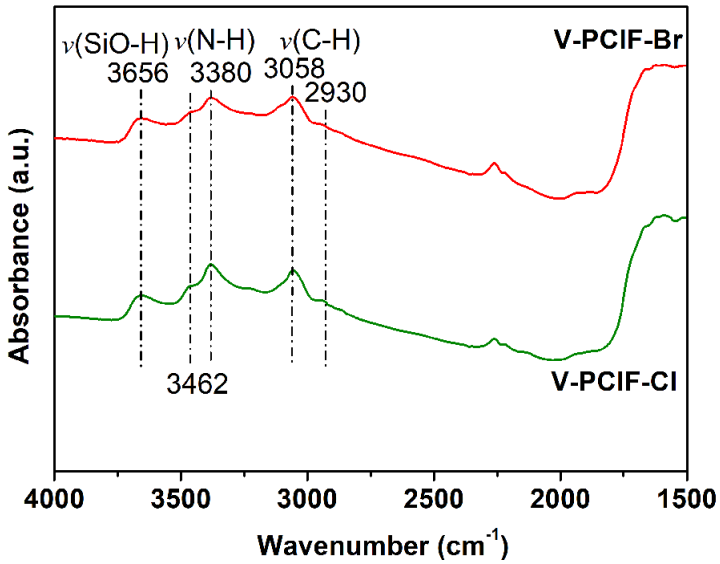


**Fig. S5** *In situ* FTIR spectra of V-PCIF-Br and V-PCIF-Cl measured at 200$^{o}$C under vacuum condition.

As shown in Fig. S5, the appearance of a broad band centered at 3656 cm$^{-1}$ is attributed to POSS-derived Si-OH, which represents at similar positions (3632 or 3630 cm$^{-1}$) measured by the common FTIR (Fig. S4C and Fig. S6). The appearance of stretching bands around 3462 and 3380 cm$^{-1}$ can be assigned to N-H stretching vibrations from the residual $NH_2$ groups in the obtained porous materials. The signals at 3058 and 2930 cm$^{-1}$ are attributed to the C-H stretching vibrations from phenyl and bipyridium rings within the formed cationic frameworks.

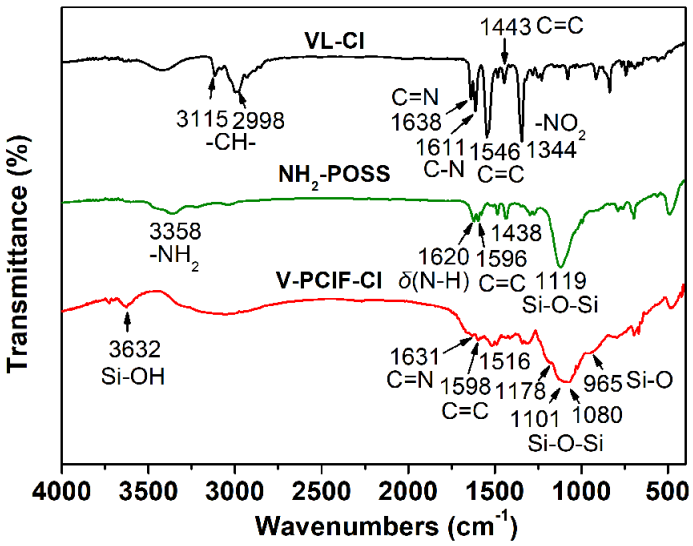


**Fig. S6** FTIR spectra of VL-Cl, $NH_2$-POSS and V-PCIF-Cl

Fig. S6 compares the FTIR of VL-Cl, $NH_2$-POSS and V-PCIF-Cl. For the viologen linker VL-Cl, the signals at 3115 and 2998 $cm^{-1}$ are attributed to C-H stretching vibrations from phenyl and bipyridium rings. The typical peaks appeared at 1638, 1546 and 1443 $cm^{-1}$ are assigned to stretching vibrations of C=N and C=C bonds from bipyridium and phenyl rings, while the sharp peaks at 1611 and 1344 $cm^{-1}$ are attributed to C-N bond and $-NO_2$ groups tethered phenyl rings. For $NH_2$-POSS, the cubic silsesquioxane cage is demonstrated by the strong peak at 1119 $cm^{-1}$ for the typical Si-O-Si asymmetric stretching vibration. The existence of $NH_2$ groups is confirmed by the N-H stretching vibration at 3358 $cm^{-1}$ and the N-H in-plane deformation vibration at 1620 $cm^{-1}$. The peaks appeared at 1596 and 1438 $cm^{-1}$ are assigned to C=C stretching vibrations from phenyl rings. After bridged with viologen linker, the obtained V-PCIF-Cl still maintains Si-O-Si structure but with the feature bands divided into three peaks 1178, 1101 and 1108 $cm^{-1}$, which is similar with V-PCIF-Br. The appearance of typical bands 1631, 1598 and 1516 $cm^{-1}$ is attributed to the C=N and C=C stretching vibrations from viologen linkers and phenyl rings. The bands at 3632 and 965 $cm^{-1}$ are assigned to the C-H and Si-O stretching vibrations derived from POSS-derived Si-OH, which is also confirmed by the *in situ* FTIR (Fig. S5).

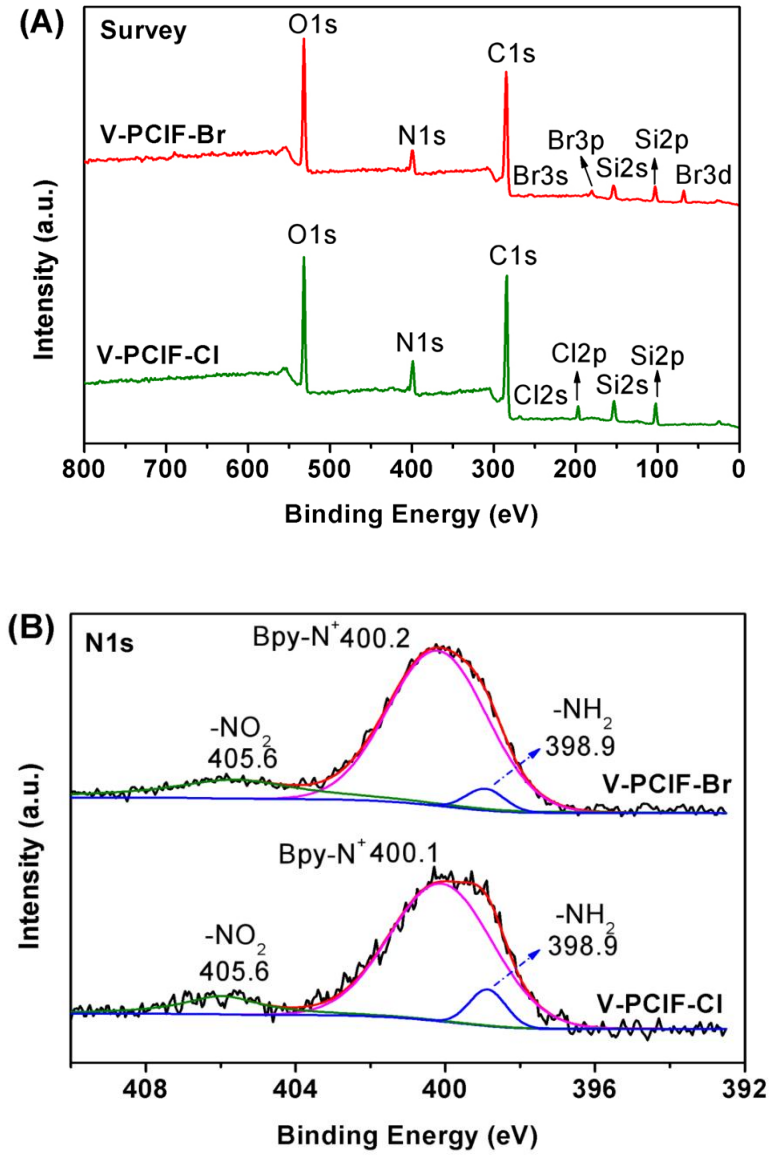


**Fig. S7** XPS (A) survey and (B) N1s core-level spectra of V-PCIF-Br and V-PCIF-Cl.

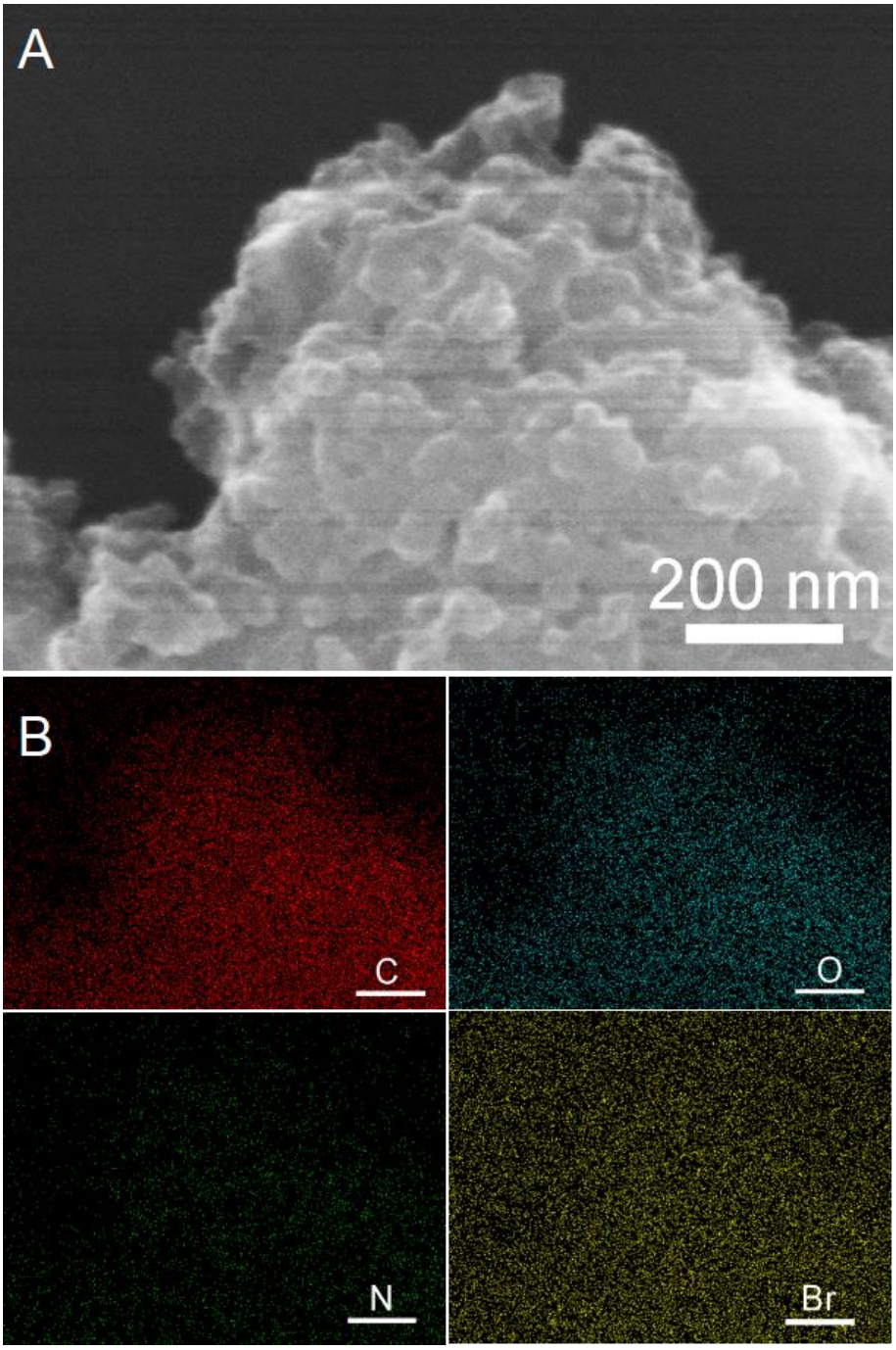


**Fig. S8** (A) SEM and (B) Energy-dispersive X-ray spectrometry (EDS) elemental mapping images including C, O, N, Br elements for the sample V-PCIF-Br (scale: 200 nm)

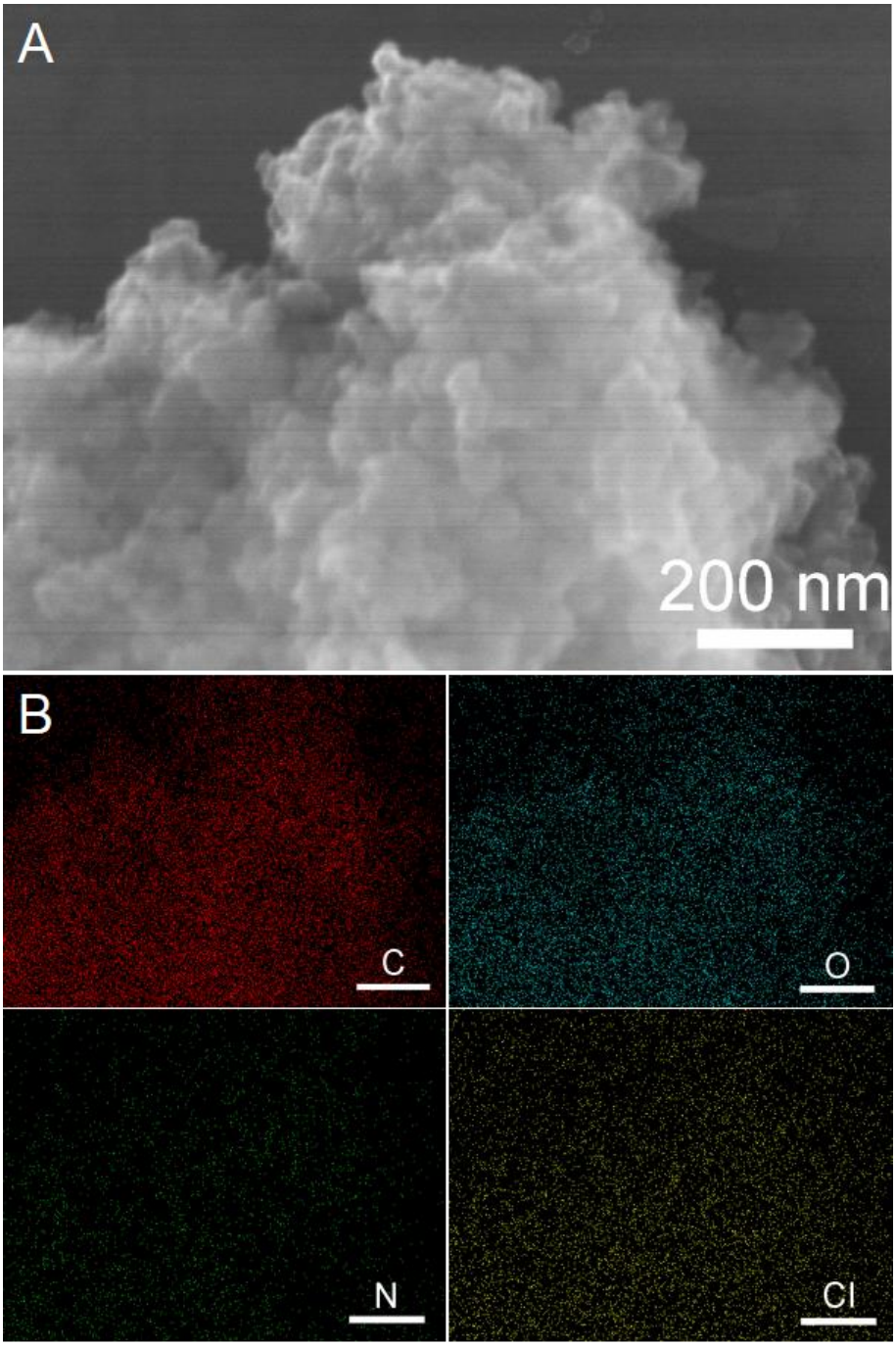


**Fig. S9** (A) SEM and (B) Energy-dispersive X-ray spectrometry (EDS) elemental mapping images including C, O, N, Cl elements for the sample V-PCIF-Cl (scale: 200 nm)

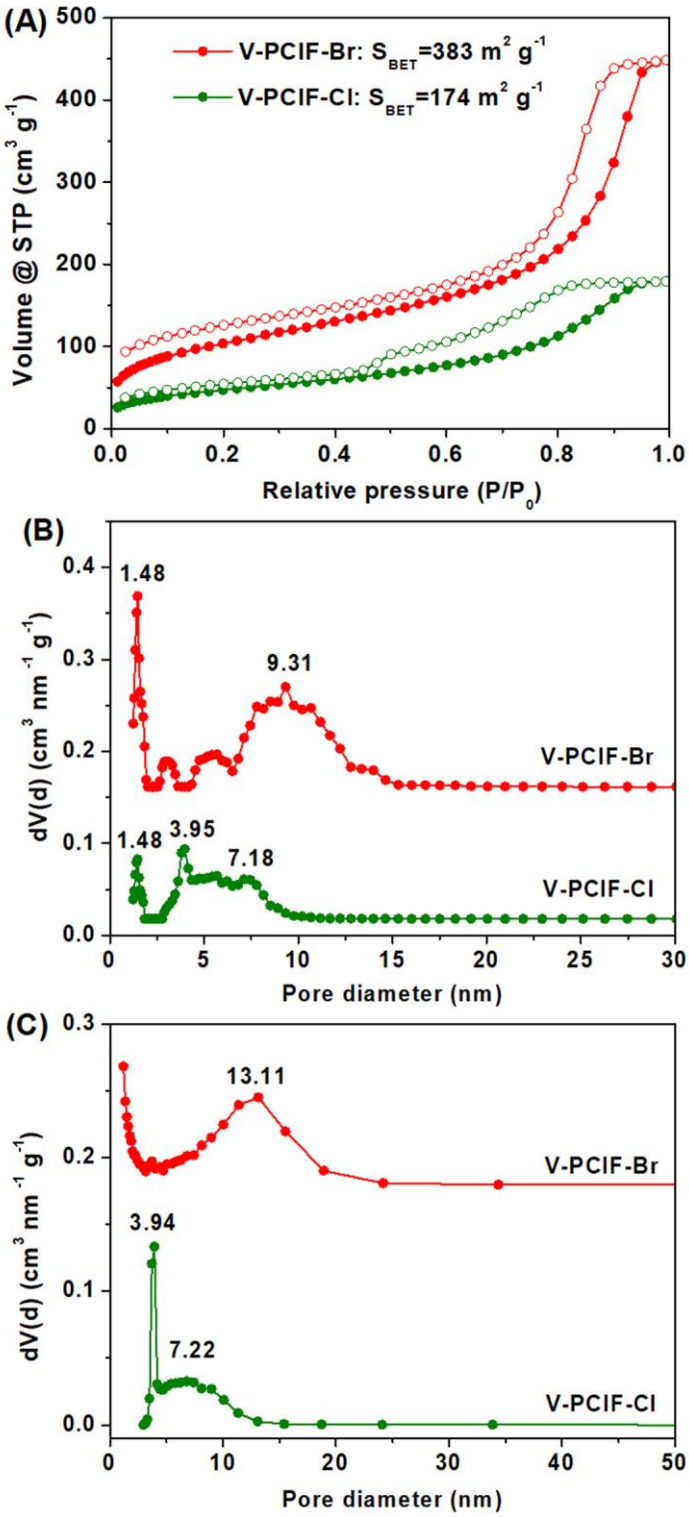


**Fig. S10** (A) $N_2$ adsorption-desorption isotherms, (B) NLDFT pore size distributions and (C) BJH pore size distributions of V-PCIF-Br and V-PCIF-Cl.

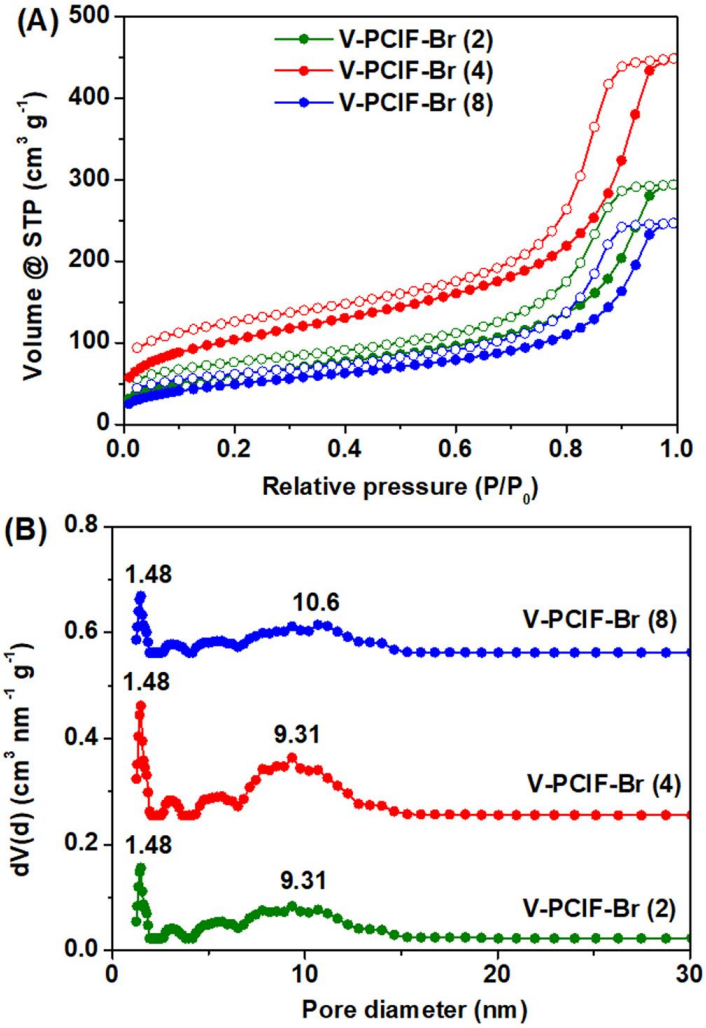


**Fig. S11** (A) $N_2$ adsorption-desorption isotherms and (B) NLDFT pore size distributions of V-PCIF-Br using different molar ratio of $NH_2$-POSS to VL-Br (*n*=2, 4, 8).

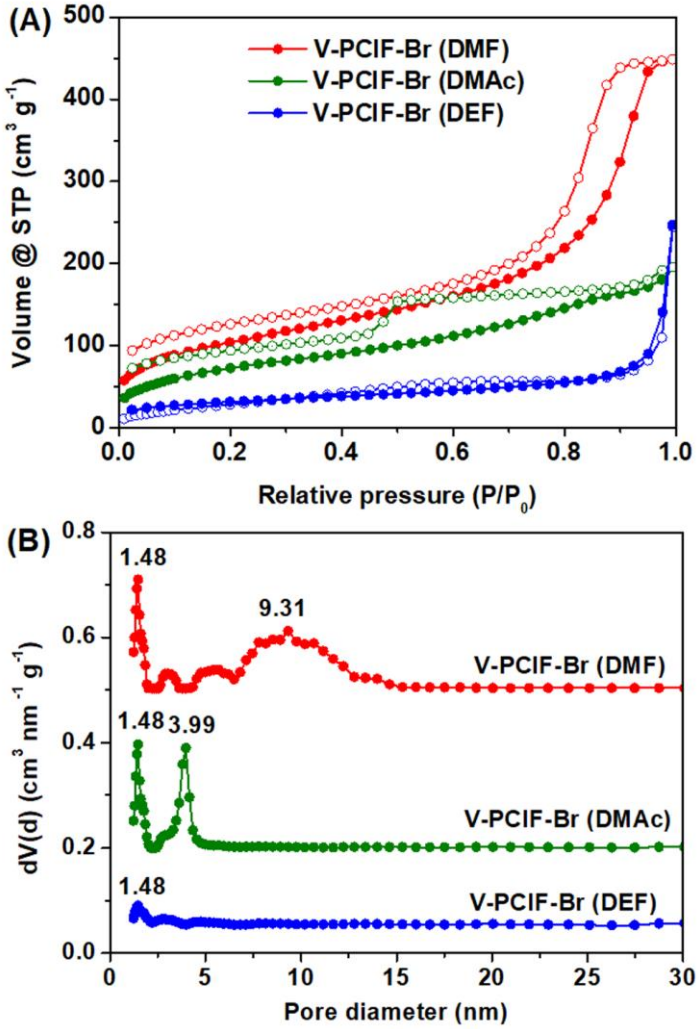


**Fig. S12** (A) $N_2$ adsorption-desorption isotherms and (B) NLDFT pore size distributions of V-PCIF-Br using different reaction solvents (DMF, DMAc and DEF).

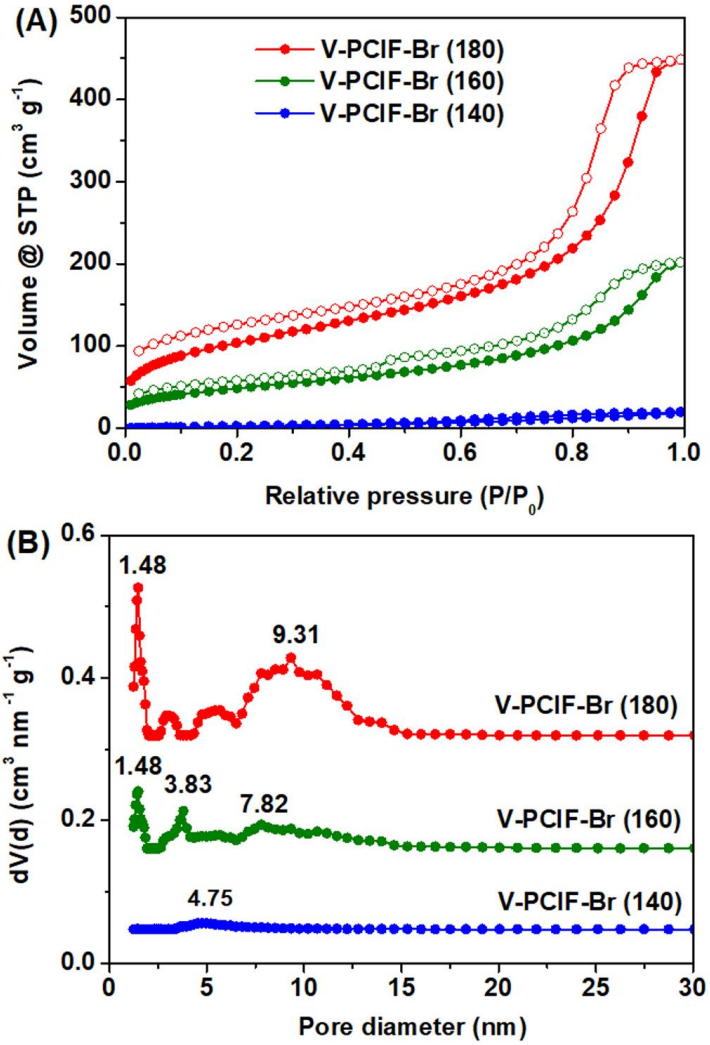


**Fig. S13** (A) $N_2$ adsorption-desorption isotherms and (B) NLDFT pore size distributions of V-PCIF-Br using different reaction temperatures (140, 160 and 180 $^{o}$C).

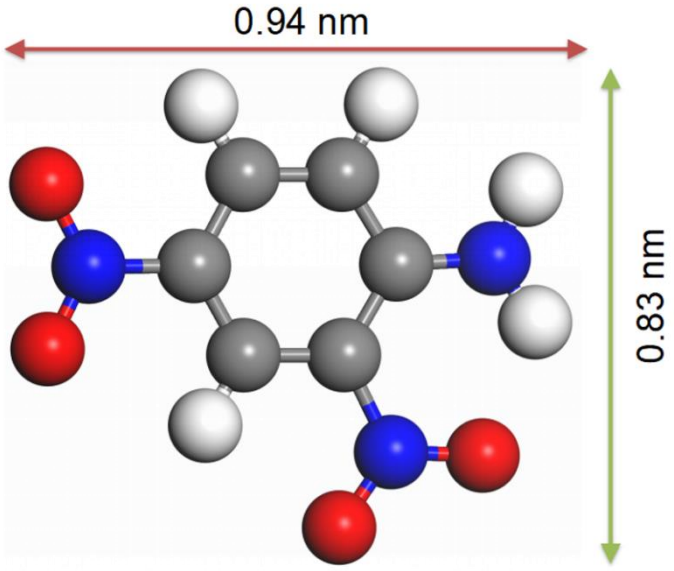


**Fig. S14** The optimized molecular structure of 2,4-dinitroaniline using material studio software.

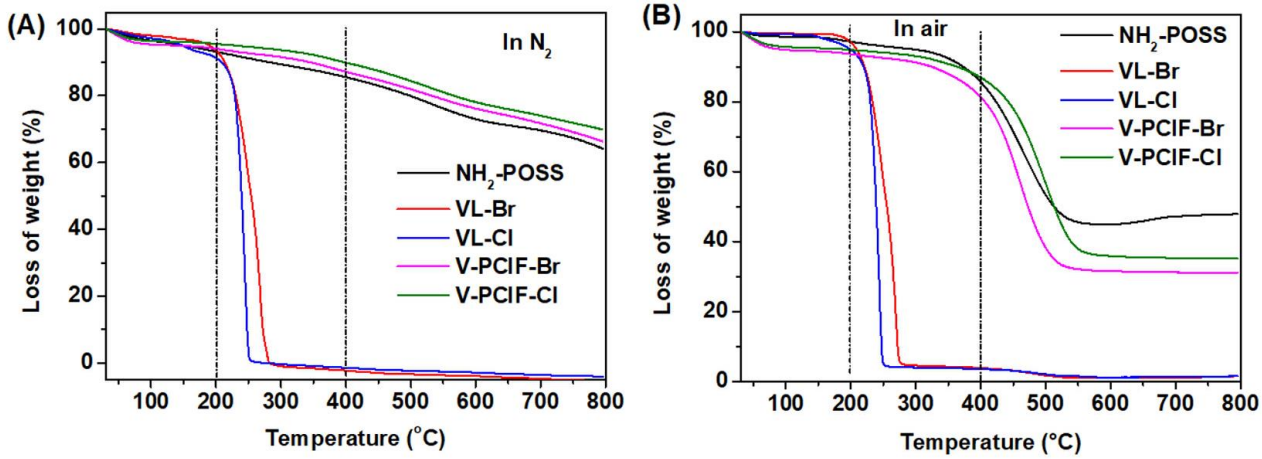


**Fig. S15** Thermogravimetric analysis (TGA) of $NH_2$-POSS, VL-X and V-PCIF-X (Cl and Br) under (A) $N_2$ and (B) air atmosphere in the range of 30 $^oC$ to 800 $^oC$ at a heating rate of 10 $^oC$ $min^{-1}$.

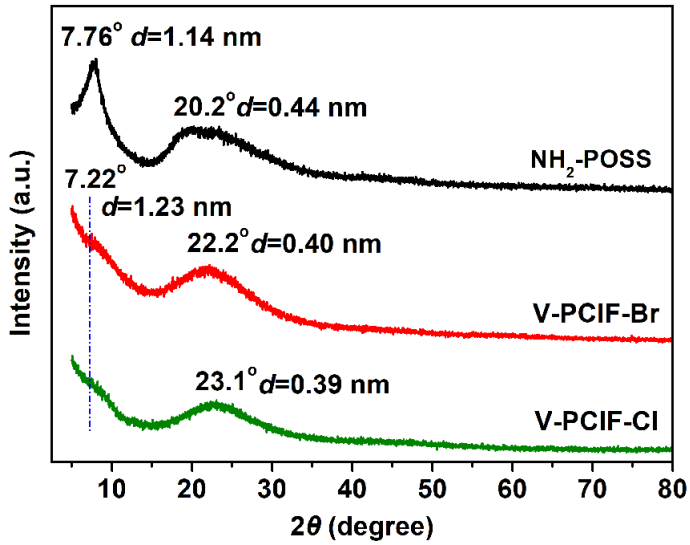


**Fig. S16** XRD patterns of $NH_2$-POSS and V-PCIF-X (X=Cl, Br).

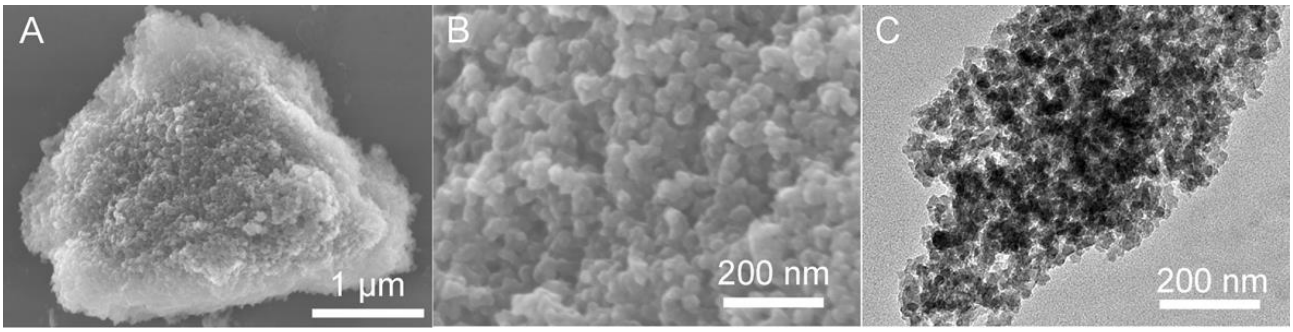


**Fig. S17** (A, B) SEM image and (C) TEM of V-PCIF-Br.

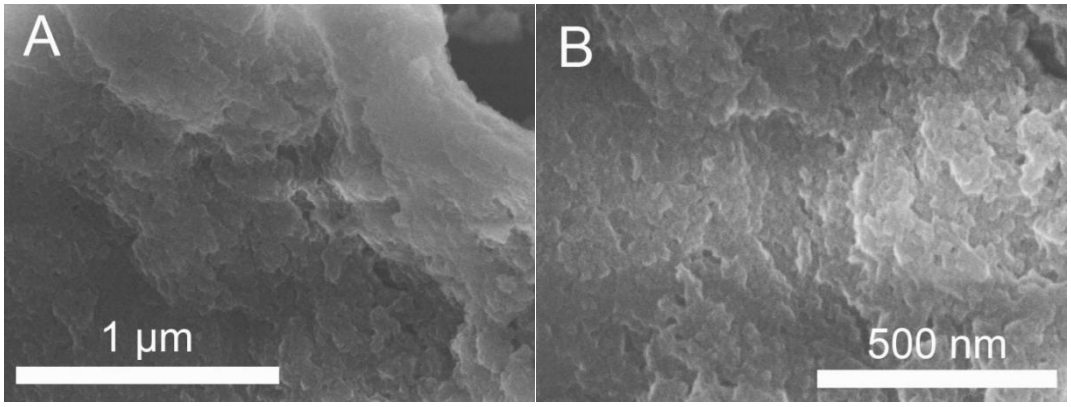


**Fig. S18** (A, B) SEM images of V-PCIF-Cl with two scales (1 μm and 500 nm).

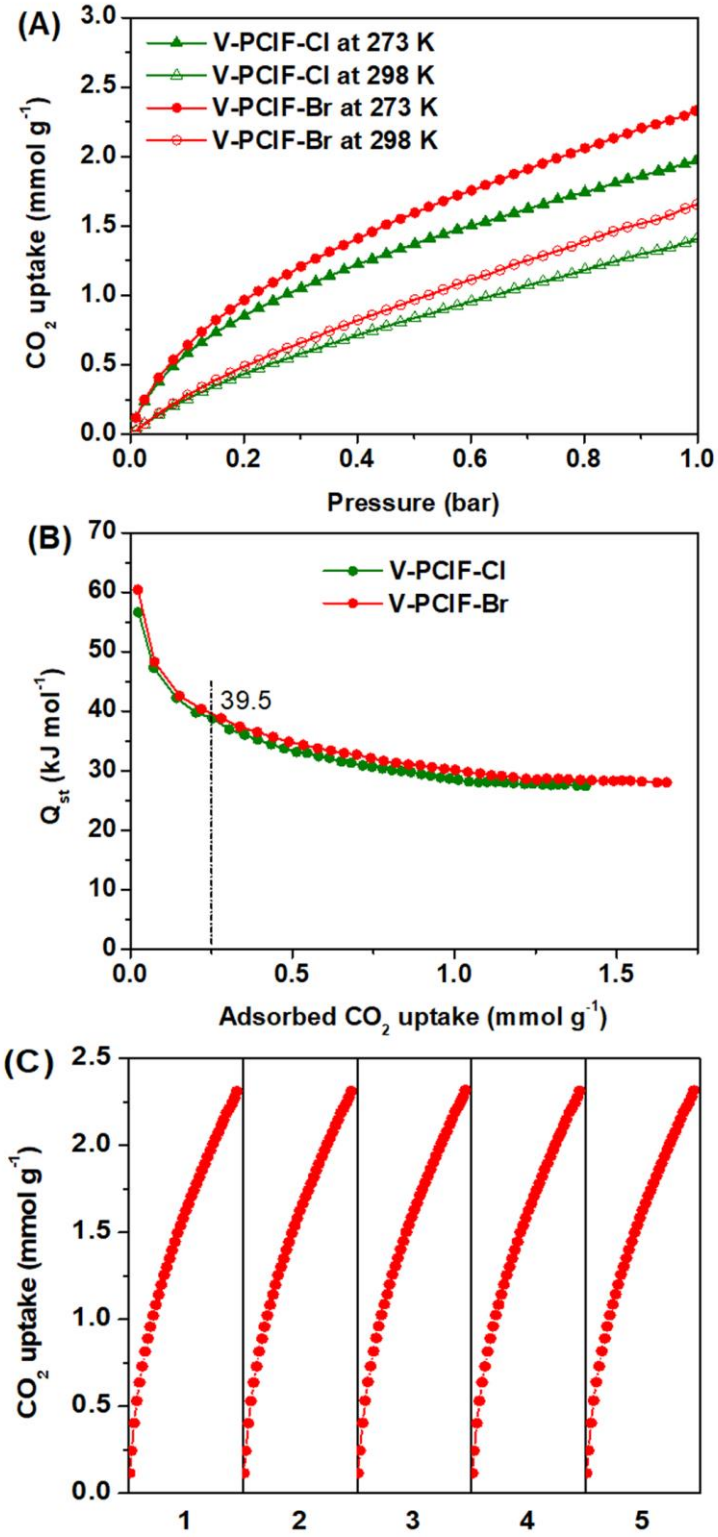


**Fig. S19** (A) $CO_2$ adsorption isotherms of V-PCIF-X (X=Cl and Br) collected up to 1.0 bar at 273 K and 298 K. (B) The isosteric heat ($Q_{st}$) plots of $CO_2$ adsorption for V-PCIF-X calculated using the Clausius-Clapeyron equation. (C) A five-cycling adsorption of $CO_2$ over the adsorbent V-PCIF-Br at 273 K by a simple regeneration under mild condition after each cycle.

The isosteric heats of adsorption ($Q_{st}$), defined as $Q_{st} = RT^2\left(\frac{\partial \ln p}{\partial T}\right)_q$, are calculated from the $CO_2$ adsorption isotherms measured at 273 and 298 K by using Clausius-Clapeyron equation and adopting the dual-site Langmuir-Freundlich (DSLF) fits (*Energy Environ. Sci*., 2011, 4, 3030; *Energy Environ. Sci*., 2015, 8, 1011; *Nat. Common*., 2017, 8,1233). Fig. S19B shows the plot of adsorption enthalpies $Q_{st}$ (kJ mol$^{-1}$) as a function of the adsorbed $CO_2$ uptakes (mmol g$^{-1}$), which presents a downward trend. At low coverage, the initial $Q_{st}$ values are high for V-PCIF-Cl (56.6 kJ mol$^{-1}$) and V-PCIF-Br (60.4 kJ mol$^{-1}$), indicative of the strong interaction between ionic frameworks and $CO_2$ molecules. With the increase of $CO_2$ uptake to 0.25 mmol g$^{-1}$, the $Q_{st}$ values present sharp decline to ca. 39 kJ mol$^{-1}$ and the values (28-30 kJ mol$^{-1}$) tend to be stable for V-PCIF-X when the ionic sites are occupied and then reach a saturation level after a certain amount of $CO_2$ (ca. 1.0 mmol g$^{-1}$). The above sharp decrease in isosteric heat of adsorption is an important result that has direct consequences for the regeneration and recycle for $CO_2$ adsorption (*Energy Environ. Sci*., 2011, 4, 3030). From the view of practical application, recyclability is an important issue. Thus, recycling adsorption of $CO_2$ over the adsorbent V-PCIF-Br at 273 K was conducted using the Quantachrome autosorb iQ2 analyzer for five cycles with no loss of adsorption capacity (Fig. S19C), which demonstrates the remarkable regeneration of V-PCIF-Br. After each adsorption cycle, V-PCIF-Br was easily regenerated under very mild conditions (60 $^{o}$C, 60 min, vacuum) in order to recover the adsorption capacity completely.

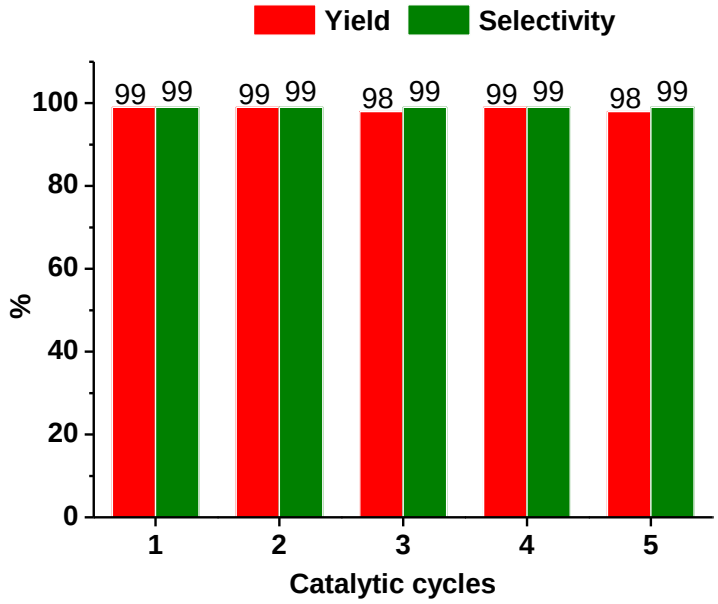


**Fig. S20** Catalytic reusability of V-PCIF-Br in the cycloaddition of $CO_2$ with epichlorohydrin. Reaction conditions: epichlorohydrin (5 mmol), $CO_2$ pressure ( 0.1 MPa), the fresh catalyst V-PCIF-Br (0.05 g), 100 $^{o}$C, 48 h.

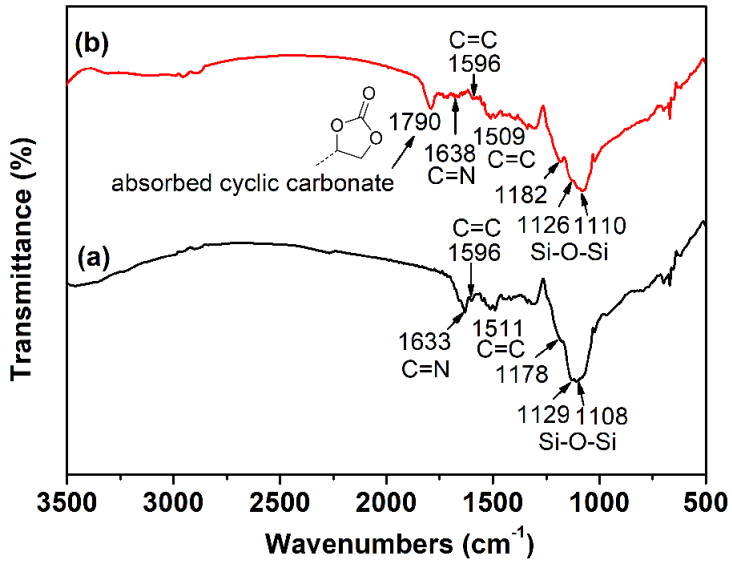


**Fig. S21** FTIR spectra of (a) the fresh catalyst V-PCIF-Br and (b) the reused V-PCIF-Br from the 5$^{th}$ recycling run.

As shown in Fig. S21, FTIR spectrum of the reused V-PCIF-Br reveals basically similar structure only with slight shifts for vibrations over the fresh one except the absorbed cyclic carbonate presented by the C=O stretching vibration at 1790 cm$^{-1}$. The divided peaks at 1182, 1126 and 1110 cm$^{-1}$ are assigned to the reserved Si-O-Si POSS cage and the signals at 1638, 1596 and 1509 cm$^{-1}$ are attributed to the C=N and C=C stretching vibrations from the existed viologen linkers and phenyl rings.

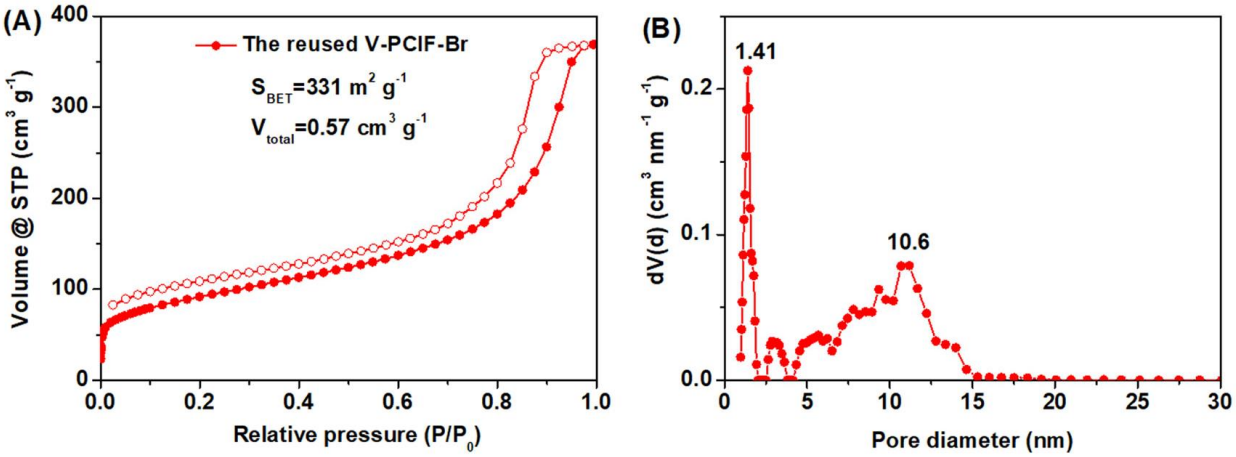


**Fig. S22** (A) $N_2$ sorption isotherms and (B) NLDFT pore size distribution of the reused catalyst V-PCIF-Br.

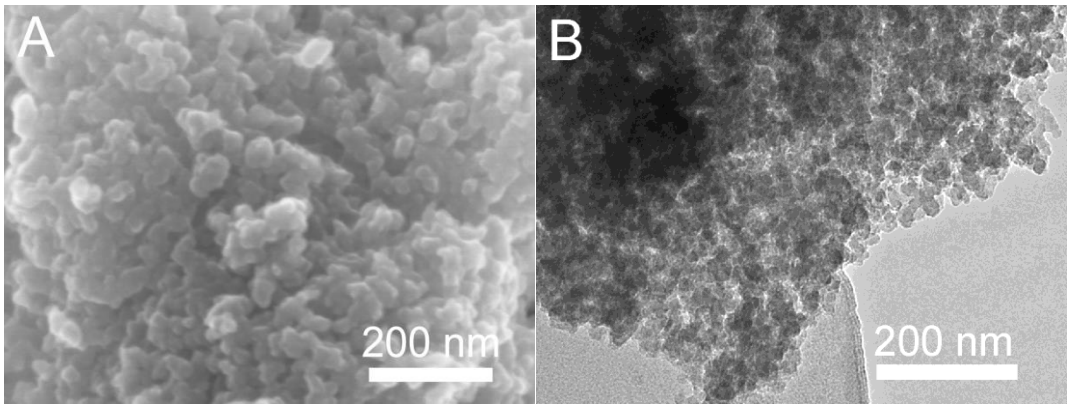


**Fig. S23** (A) SEM image and (B) TEM image of the the reused catalyst V-PCIF-Br.

**Table S1** Textural properties of V-PCIFs series using two viologen linkers with different halogen anions.[a]

| Samples | Ionic linkers | $S_{BET}$ ($m^2$ $g^{-1}$) [b] | $V_{total}$ ($cm^3$ $g^{-1}$) [c] | $D_p$ (nm) [d] | N content (mmol $g^{-1}$) [e] | $CO_2$ uptake (mmol $g^{-1}$) [f] | |
|---|---|---|---|---|---|---|---|
| | | | | | | 273 K | 298K |
| V-PCIF-Br | VL-Br | 383 | 0.70 | 1.48, 9.31 | 6.35 | 2.33 | 1.66 |
| V-PCIF-Cl | VL-Cl | 174 | 0.28 | 1.48, 3.96 | 7.25 | 1.97 | 1.41 |

[a] Reaction conditions: $NH_2$-POSS (0.05 mmol), VL-Br or VL-Cl (0.2 mmol), solvent DMF (10 mL), 180 $^oC$, 48 h. [b] BET surface area calculated over the range $P/P_0$=0.05~0.20. [c] Total pore volume calculated at $P/P_0$=0.99. [d] The peak pore diameter calculated by the NLDFT theory. [e] The N content calculated by CHN elemental analysis. [f] $CO_2$ uptakes were measured at 273 and 298 K, 1.0 bar.

**Table S2** Textural properties of V-PCIF-Br series using different molar ratio of $NH_2$-POSS to VL-Br.[a]

| Samples | $n$($NH_2$-POSS):$n$(VL-Br) | $S_{BET}$ ($m^2$ $g^{-1}$) [b] | $V_{total}$ ($cm^3$ $g^{-1}$) [c] | $D_p$ (nm) [d] |
|---|---|---|---|---|
| V-PCIF-Br (2) | 1:2 | 221 | 0.46 | 1.48, 9.31 |
| V-PCIF-Br (4) | 1:4 | 383 | 0.70 | 1.48, 9.31 |
| V-PCIF-Br (8) | 1:8 | 182 | 0.38 | 1.48, 10.6 |

[a] Reaction conditions: $NH_2$-POSS (0.05 mmol), VL-Br (0.1~0.4 mmol), solvent DMF (10 mL), 180 $^oC$, 48 h. [b] BET surface area calculated over the range $P/P_0$=0.05~0.20. [c] Total pore volume calculated at $P/P_0$=0.99. [d] The peak pore diameter calculated by the NLDFT theory.

By varying the molar ratios of $NH_2$-POSS to VL-Br from 1:2 to 1:8 (see Fig. S11 and Table S2), the obtained V-PCIF-Br ($n$=2, 4, 8) samples possess distinct $S_{BET}$ values of 221, 383 and 182 $m^2$ $g^{-1}$, indicating the optimal proportion is based on stoichiometric ratio (1:4). We found that high-boilling amides solvents (i.e. DMF, DMAc and DEF) are more suitable for affording high-surface-area V-PCIF-Br series (Fig. S12 and Table S3), offering $S_{BET}$ values of 383, 270 and 120 $m^2$ $g^{-1}$ in DMF, DMAc and DEF, respectively, while the low-boilling solvents ethanol/water, dioxane and acetonitrile only give low-surface-area solids (< 20 $m^2$ $g^{-1}$). No solid was obtained in high-boilling solvent DMSO. Besides, $S_{BET}$ values of V-PCIF-Br (Fig. S13 and Table S4) are determined by different temperatures in DMF: V-PCIF-Br has a low surface area of 19 $m^2$ $g^{-1}$; V-PCIF-Br has a moderate surface area of 176 $m^2$ $g^{-1}$ at a higher temperature 160 $^oC$ ; at a high temperature 180 $^oC$ dramatically affords the highest surface area of 383 $m^2$ $g^{-1}$ for V-PCIF-Br.

**Table S3** Textural properties of V-PCIF-Br influenced by different reaction solvents.[a]

| Samples | Solvent | $S_{BET}$ ($m^2$ $g^{-1}$) [b] | $V_{total}$ ($cm^3$ $g^{-1}$) [c] | $D_p$ (nm) [d] |
|---|---|---|---|---|
| V-PCIF-Br (DMF) | DMF | 383 | 0.70 | 1.48, 9.31 |
| V-PCIF-Br (DMAc) | DMAc | 270 | 0.30 | 1.48, 3.99 |
| V-PCIF-Br (DEF) | DEF | 120 | 0.38 | 1.48 |

[a] Reaction conditions: $NH_2$-POSS (0.05 mmol), VL-Br (0.2 mmol), solvent (10 mL), 180 $^oC$, 48 h. [b] BET surface area calculated over the range $P/P_0$=0.05~0.20. [c] Total pore volume calculated at $P/P_0$=0.99. [d] The peak pore diameter calculated by the NLDFT theory.

**Table S4** Textural properties of V-PCIF-Br influenced by different reaction temperature.[a]

| Samples | Temperature ($^oC$) | $S_{BET}$ ($m^2$ $g^{-1}$) [b] | $V_{total}$ ($cm^3$ $g^{-1}$) [c] | $D_p$ (nm) [d] |
|---|---|---|---|---|
| V-PCIF-Br (140) | 140 | 19 | 0.03 | 4.75 |
| V-PCIF-Br (160) | 160 | 176 | 0.31 | 1.48, 3.83, 7.82 |
| V-PCIF-Br (180) | 180 | 383 | 0.70 | 1.48, 9.31 |

[a] Reaction conditions: $NH_2$-POSS (0.05 mmol), VL-Br (0.2 mmol), solvent (10 mL), 140~180 $^oC$, 48 h. [b] BET surface area calculated over the range $P/P_0$=0.05~0.20. [c] Total pore volume calculated at $P/P_0$=0.99. [d] The peak pore diameter calculated by the NLDFT theory.

**Table S5** $CO_2$ adsorption performance of POSS-based porous polymers and various porous ionic polymers and other typical porous adsorbents.

| Type | Sample | $S_{BET}$ ($m^2$ $g^{-1}$) | $CO_2$ uptake (mmol $g^{-1}$) | | Ref. |
|---|---|---|---|---|---|
| | | | 273 K, 1.0 bar | 298 K, 1.0 bar | |
| Neutral POSS-based porous polymer | HPP-3 | 805 | 1.38 | 0.68 | S4 |
| | HPP-1c | 650 | 1.56 | 0.86 | S5 |
| | THPP | 915 | 1.16 | - | S6 |
| | HLPP-3 | 841 | 0.75 | - | S7 |
| | FHPP-1 | 602 | 0.74 | - | S8 |
| Porous ionic polymers | PCIF-1(M4) | 942 | 0.96 | 0.68 | S9 |
| | PCP-Cl | 755 | 2.31 | 1.40 | S10 |
| | red-POP-V2 | 591 | - | 1.09 | S11 |
| | cCTF-500 | 1247 | 3.02 | 1.82 | S12 |
| | CCTF-500 | 1353 | - | 1.94 | S13 |
| | PIP-Bn-Cl | 758 | 2.23 | 1.52 | S14 |
| | POM2-IM | 653 | 3.3 | - | S15 |
| | Polymer-4 | 852 | 2.9 | 1.7 | S16 |
| | HCP-IL-8 | 450 | 1.7 | 1.2 | S17 |
| | CB-PCP-1 | 419 | 2.05 | 1.2 | S18 |
| | PDMBr | 205 | 1.02 | - | S19 |
| | PDBA-Cl-SCD | 211 | 1.03 | - | S20 |
| | PVIm-6-SCD | 797.7 | 3.60 | - | S21 |
| | HIP-Br-2 | 534 | 2.9 | 1.9 | S22 |
| | CPN-1-Cl | 1504 | 2.85 | - | S23 |
| | **V-PCIF-Cl** | **174** | **1.97** | **1.41** | **This work** |
| | **V-PCIF-Br** | **383** | **2.33** | **1.66** | **This work** |
| Other typical adsorbents (zeolites, MOFs and carbons) [a] | NaX Zeolite | 600 | - | 4.98 | S24 |
| | 13X Zeolite | 800 | - | 4.7 | S25, S26 |
| | FJI-H14 | 904 | - | 6.44 | S27 |
| | MAF-X25ox | 1286 [b] | - | 7.1 | S28 |
| | MAF-X27ox | 1167 [b] | - | 6.7 | S28 |
| | $Co_2$(dobdc) | 1080 | - | 6.9 | S29 |
| | Mg-MOF-74 | 1495 | - | 8.0 | S29 |
| | PCN-14 | 918 | 5.33 | 3.68 | S30 |
| | CEM750 | 3360 | 6.92 | 4.38 | S31 |

[a] Other typical adsorbents relates to zeolites (NaX and 13X zeolite), MOFs (FJI-H14, MAF-X25ox, MAF-X27ox, $Co_2$(dobdc) and Mg-MOF-74) and porous carbons (PCN-14 and CEM750). [b] Langmuir surface areas.

**Table S6** Catalytic activities of different ionic sites-containing organic polymers heterogeneous catalysts for metal-free cycloaddition of $CO_2$ with epichlorohydrin without adding any co-catalysts.

| Catalyst | $CO_2$ pressure (MPa) | Temperature ($^oC$) | Time (h) | Yield (%) | Ref. |
|---|---|---|---|---|---|
| PCP-Cl | 3 | 100 | 12 | 98 | S10 |
| IT-POP-1 | 1 | 120 | 10 | 99 | S32 |
| poly-imidazoliums | 1 | 110 | 2 | 94 | S33 |
| POM3-IM | 1 | 120 | 8 | 90 | S15 |
| cCTF-500 | 1 | 90 | 12 | 95 | S12 |
| FIP-Im | 1 | 80 | 10 | 99 | S34 |
| CCTF-350 | 0.1 | 120 | 24 | 93.1 | S13 |
| PIP-Bn-Cl | 0.1 | 100 | 3 | 99 | S14 |
| PDMBr | 0.1 | 120 | 12 | 91.3 | S19 |
| IP3 | 0.1 | 100 | 24 | 99 | S35 |
| PDBA-Cl-SCD | 0.1 | 90 | 6 | 99.3 | S20 |
| PGDBr-5-2OH | 0.1 | 70 | 24 | 91 | S36 |
| HIP-Br-2 | 0.1 | 120 (70) | 48 (96) | 90 | S22 |
| **V-PCIF-Br** | **1** | **100 (80)** | **6 (12)** | **98 (94)** | **This work** |
| **V-PCIF-Br** | **0.1** | **100 (80)** | **48 (72)** | **99 (97)** | **This work** |

**Table S7** Catalytic activities of some typical efficient catalysts for cycloaddition of $CO_2$ with epichlorohydrin by adding the co-catalyst TBAB.

| Type | Catalyst | Co-catalyst | $CO_2$ pressure (MPa) | Temperature ($^oC$) | Time (h) | Yield (%) | Ref. |
|---|---|---|---|---|---|---|---|
| Metal-based POPs | Co/POP-TPP | TBAB [a] | 0.1 | 29 | 24 | 94.6 | S37 |
| | Cu/POP-Bpy | TBAB | 0.1 | 29 | 48 | 99 | S38 |
| | HUST-1-Co | TBAB | 0.1 | 25 | 48 | 94.7 | S39 |
| MOFs | Zn-MOF 1´[b] | TBAB | 0.1 | 80 | 2 | 89 | S40 |
| | Ba-MOF 1a [c] | TBAB | 0.1 | 25 | 48 | 90 | S41 |
| | Cu-MOF [d] | TBAB | 0.1 | 25 | 48 | 88 | S42 |

[a] tetra-*n*-butyl-ammonium bromide (TBAB).

[b] Zn-MOF 1´is the desolvated sample of $[Zn_2(L)(2,6\text{-}NDC)_2(H_2O)]\cdot 1.5DMF\cdot 2H_2O$ (1).

[c] Ba-MOF 1a is the guest-free phase of $\{[Ba_2(BDPO)(H_2O)]\cdot DMA\}_n$ (1).

[d] Cu-MOF is $\{Cu_2[(C_{20}H_{12}N_2O_2)(COO)_4]\}_n$.

**Table S8** Cycloaddition of $CO_2$ with various epoxides catalyzed by V-PCIF-Br.[a]

| Entry | Substrate | Product | *T* (°C) | *P* (MPa) | *t* (h) | *Yield* (%)[b] | Selectivity (%)[b] |
|---|---|---|---|---|---|---|---|
| 1 | 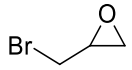 | 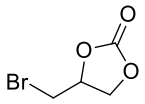 | 100 | 1 | 6 | 99 | 99 |
| | | | 100 | 0.1 | 48 | 98 | 99 |
| | | | 80 | 0.1 | 72 | 98 | 99 |
| 2 | 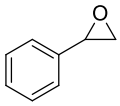 | 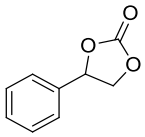 | 100 | 1 | 6 | 98 | 99 |
| | | | 100 | 0.1 | 48 | 96 | 99 |
| | | | 80 | 0.1 | 72 | 92 | 99 |
| 3 | 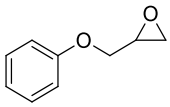 | 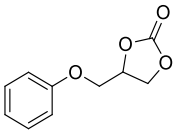 | 100 | 1 | 6 | 96 | 99 |
| | | | 100 | 0.1 | 48 | 94 | 99 |
| | | | 80 | 0.1 | 72 | 93 | 99 |
| 4 | 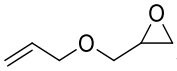 | 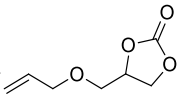 | 100 | 1 | 6 | 95 | 99 |
| | | | 120 | 0.1 | 48 | 96 | 99 |
| | | | 80 | 0.1 | 72 | 90 | 99 |
| 5 | 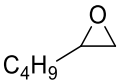 | 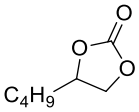 | 100 | 1 | 6 | 96 | 99 |
| | | | 120 | 0.1 | 48 | 99 | 99 |
| | | | 80 | 0.1 | 72 | 92 | 99 |

[a] Reaction conditions: epoxide (5 mmol), catalyst V-PCIF-Br (0.05 g, 3 mol% based on VL), $CO_2$ pressure (*P*=1 MPa or 0.1 MPa), temperature (*T*=80~120 °C), time (*t*=6~72 h).[b] Yield and selectivity of the cyclic carbonate determined by GC and $^1$HNMR.

The scope of epoxide substrates is explored over V-PCIF-Br for the cycloaddition of $CO_2$ under both 1 MPa and 0.1 MPa $CO_2$ pressure. As summarized in Table S8, high yields (96-99%) for all of the target cyclic carbonates are obtained at 100 °C for 6 h under 1 MPa $CO_2$ pressure over various substrates including the terminal epoxides (epibromohydrin, styrene oxide, glycidyl phenyl ether, allyl glycidyl ether and 2-butyloxirane) with both electron withdrawing and electron-donating substituents. These substrates can be converted into the corresponding cyclic carbonates with high yields (94-99%) under atmospheric pressure, at temperatures of 100-120 °C for 48 h. With a prolonged reaction time to 72 h, the desired yields (90-98%) are obtained at a low temperature of 80 °C over the above epoxides including inert epoxides containing phenyl groups (entries 2 and 3) and the less reactive aliphatic long carbon-chain alkyl epoxide (entry 5). Obviously, V-PCIF-Br exhibits remarkable catalytic activities toward various epoxides under mild conditions, indicative of good substrate compatibility.

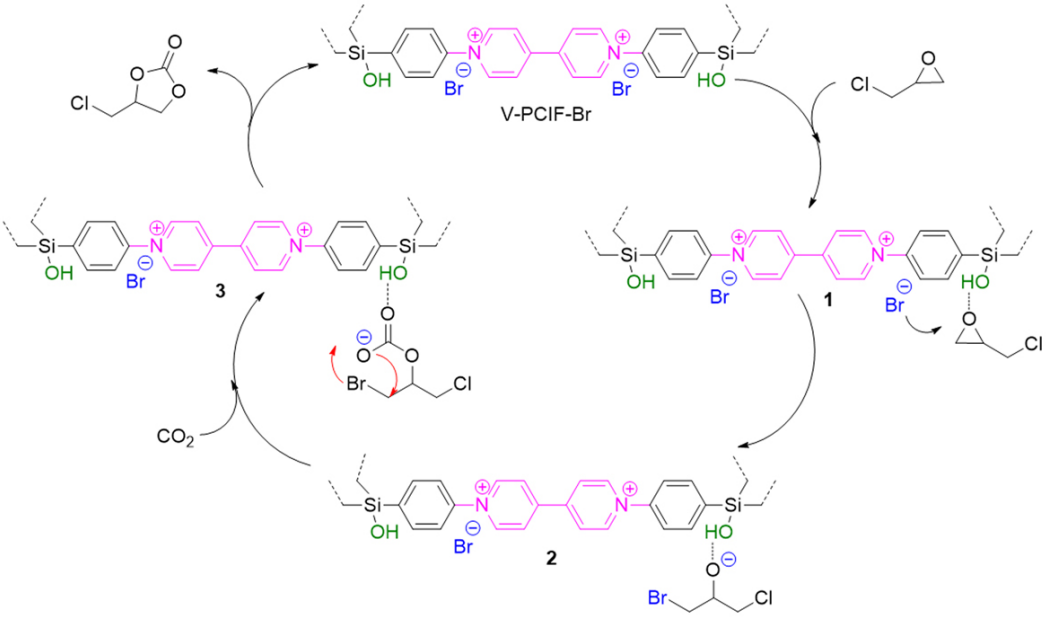


**Scheme S4** The proposed catalytic reaction process for the fixation of $CO_2$ with epichlorohydrin into the targeted cyclic carbonate catalyzed by V-PCIF-Br.

**References**


S1 F. Biedermann and O. A. Scherman, *J. Phys. Chem. B*, 2012, **116**, 2842.

S2 C. Eaborn, *Pure Appl. Chem*., 1969, **19**, 375.

S3 R. H. Krieble and J. R Elliott, *J. Am. Chem. Soc*., 1946, **68**, 2291.

S4 D. Wang, W. Yang, S. Feng and H. Liu, *Polym. Chem*., 2014, **5**, 3634.

S5 D. Wang, S. Feng and H. Liu, *Chem. Eur. J*., 2016, **22**, 14319.

S6 M. Ge and H. Liu, *J. Mater. Chem. A*, 2016, **4**, 16714.

S7 R. Shen, Y. Liu, W. Yang, Y. Hou, X. Zhao and H. Liu, *Chem. Eur. J*., 2017, **23**, 13465.

S8 M. Ge and H. Liu, *Chem. Eur. J*., 2018, **24**, 2224.

S9 G. Chen, Y. Zhou, X. Wang, J. Li, S. Xue, Y. Liu, Q. Wang and J. Wang, *Sci. Rep*., 2015, **5**, 11236.

S10 O. Buyukcakir, S. H. Je, D. S. Choi, S.N. Talapaneni, Y. Seo, Y. Jung, K. Polychronopoulouc and A. Coskun, *Chem. Commun*., 2016, **52**, 934.

S11 C. Hua, B. Chan, A. Rawal, F. Tuna, D. Collison, J. M. Hook and D. M. D'Alessandro, *J. Mater. Chem. C*, 2016, **4**, 2535.

S12 O. Buyukcakir, S. H. Je, S. N. Talapaneni, D. Kim and A. Coskun, *ACS Appl. Mater. Interfaces*, 2017, **9**, 7209.

S13 T.-T. Liu, R. Xu, J.-D. Yi, J. Liang, X.-S. Wang, P.-C. Shi, Y.-B. Huang and R. Cao, *ChemCatChem*, 2018, **10**, 2036.

S14 Q. Sun,Y. Jin, B. Aguila, X. Meng, S. Ma and F.-S. Xiao, *ChemSusChem*, 2017, **10**, 1160.

S15 J. Wang, W. Sng, G. Yi and Y. Zhang, *Chem. Commun*., 2015, **51**, 12076.

S16 J. Wang, J. G. W. Yang, G. Yi and Y. Zhang, *Chem. Commun*., 2015, **51**, 15708.

S17 L. Hu, H. Ni, X. Chen, L. Wang, Y. Wei, T. Jiang, Y. Lu, X. Lu and P. Ye, *Polym. Eng. Sci*., 2016, **56**, 573.

S18 A. Dani, V. Crocellà, C. Magistris, V. Santoro, J. Yuan and S. Bordiga, *J. Mater. Chem. A*, 2017, **5**, 372.

S19 X. Wang, Y. Zhou, Z. Guo, G. Chen, J. Li, Y. Shi, Y. Liu and J. Wang, *Chem. Sci*., 2015, **6**, 6916.

S20 Y. Xie, Q. Sun, Y. Fu, L. Song, J. Liang, X. Xu, H. Wang, J. Li, S. Tu, X. Lu and J. Li, *J. Mater. Chem. A*, 2017, **5**, 25594.

S21 Y. Xie, J. Liang, Y. Fu, M. Huang, X. Xu, H. Wang, S. Tu and J. Li, *J. Mater. Chem. A*, 2018, **6**, 6660.

S22 J. Li, D. Jia, Z. Guo, Y. Liu, Y. Lyu, Y. Zhou and J. Wang, *Green Chem*., 2017, **19**, 2675.

S23 S. Fischer, A. Schimanowitz, R. Dawson, I. Senkovska, S. Kaskel and A. Thomas, *J. Mater. Chem. A*, 2014, **2**, 11825.

S24 K. S. Walton, M. B. Abney, M. D. LeVan, *Micropor. Mesopor. Mater.*, 2006, **91**, 78.

S25 S. Cavenati, C. A. Grande and A. E. Rodrigues, *J. Chem. Eng. Data*, 2004, **49**, 1095.

S26 R. S. Franchi, P. J. E. Harlick and A. Sayari, *Ind. Eng. Chem. Res*., 2005, **44**, 8007.

S27 L. Liang, C. Liu, F. Jiang, Q. Chen, L. Zhang, Hui Xue, H.-L. Jiang,J. Qian, D. Yuan and M. Hong, *Nat. Common*., 2017, **8**,1233.

S28 P.-Q. Liao, H. Chen, D.-D. Zhou, S.-Y. Liu, C.-T. He, Z. Rui, H. J, J.-P. Zhang and X.-M. Chen, *Energy Environ. Sci*., 2015, **8**, 1011.

S29 S. R. Caskey, A. G. Wong-Foy and A. J. Matzger, *J. Am. Chem. Soc*., 2008, **130**, 10870.

S30 G. Chen, X. Wang, J. Li, W. Hou, Y. Zhou and J. Wang, *ACS Appl. Mater. Interfaces*, 2015, **7**, 18508.

S31 Y. Xia, R.Mokaya, G. S. Walker and Y. Zhu, *Adv. Energy Mater*., 2011, **1**, 678.

S32 H. Zhong, Y. Su, X. Chen, X. Li, R. Wang, *ChemSusChem*, 2017, **10**, 4855.

S33 J. Wang, J. Leong and Y. Zhang, *Green Chem*., 2014, **16**, 4515.

S34 Y. Chen, R. Luo, J. Bao, Q. Xu, J. Jiang, X. Zhou and H. Ji, *J. Mater. Chem. A*, 2018, **6**, 9172.

S35 W. Zhong, F. D. Bobbink, Z. Fei and P. J. Dyson, *ChemSusChem*, 2017, **10**, 2728.

S36 Z. Guo, Q. Jiang, Y. Shi, J. Li, X. Yang, W. Hou, Y. Zhou and J. Wang, *ACS Catal*., 2017, **7**, 6770.

S37 Z. Dai, Q. Sun, X. Liu, C. Bian, Q. Wu, S. Pan, L. Wang, X. Meng, F. Deng, F.-S. Xiao, *J. Catal*., 2016, **338**, 202.

S38 Z. Dai, Q. Sun, X. Liu, L. Guo, J. Li, S. Pan, C. Bian, X. Hu, X. Meng, L. Zhao, F. Deng, F.-S. Xiao, *ChemSusChem*, 2017, **10**, 1186.

S39 S. Wang, K. Song, C. Zhang, Y. Shu, T. Li and B. Tan, *J. Mater. Chem. A*, 2017, **5**, 509.

S40 D. Zhao, X.-H. Liu, J.-H. Guo, H.-J. Xu, Y. Zhao, Y. Lu and W.-Y. Sun, *Inorg. Chem*., 2018, **57**, 2695.

S41 X.-Y. Li, L.-N.Ma, Y. Liu, L. Hou, Y.-Y. Wang and Z. Zhu, *ACS Appl. Mater. Interfaces*, 2018, **10**, 10965.

S42 P.-Z. Li, X.-J. Wang, J.Liu, H. S. Phang, Y. Li and Y. Zhao, *Chem. Mat*er., 2017, **29**, 9256.